buildings

MDPI

Article

Thermal Analysis of Air-Cooled Channels of Different Sizes in Naturally Ventilated Photovoltaic Wall Panels

Yongxiao Zheng [1], Jikui Miao [1,*], Hongwen Yu [1], Fang Liu [2] and Qingfeng Cai [2]

[1] School of Architecture and Urban Planning, Shandong Jianzhu University, Jinan 250101, China; 2021050230@stu.sdjzu.edu.cn (Y.Z.); 24239@sdjzu.edu.cn (H.Y.)
[2] School of Thermal Engineering, Shandong Jianzhu University, Jinan 250101, China; fliu@sdjzu.edu.cn (F.L.); 2021030205@stu.sdjzu.edu.cn (Q.C.)
* Correspondence: mjikui2004@sdjzu.edu.cn

Abstract: In practical engineering applications, natural air cooling is often utilized for photovoltaic (PV) facades. However, the natural-air-cooling method is not effective at cooling PV wall panels, and the high temperatures accumulated on the surface of PV panels not only affect the electrical efficiency and service life of the PV modules, but also increase the energy consumption of the building. In this paper, we propose the vertical installation of heat dissipation fins in naturally ventilated PV wall panels. We used ANSYS Fluent to establish the simulation model of naturally ventilated PV wall panels and validate it. By simulating the air-cooled channels in PV wall panels with different sizing parameters, the temperature and flow rate variations were comparatively analyzed in order to optimize the air-cooled-channel sizes. The results show that installing the fins vertically in the air-cooled channel provided better cooling for the PV panels and enhanced the air heat collection effect. Additionally, it improved the airflow rate in the channel. As the thickness of the finned air-cooled channel increased or the width decreased, the temperature on the surface of the PV panels showed a decreasing trend. Compared to the flat-plate air-cooled channel, the finned air-cooled channel, with a thickness of 100 mm and a width of 20 mm, decreased the peak and average temperatures of the PV-panel surface by 3.9 °C and 8.1 °C, respectively, and increased the average temperature of the air at the outlet by 11.2 °C.

Keywords: cooling fins; natural ventilation; photovoltaic wall panels; air-cooled channels; thermal analysis

check for updates

Citation: Zheng, Y.; Miao, J.; Yu, H.; Liu, F.; Cai, Q. Thermal Analysis of Air-Cooled Channels of Different Sizes in Naturally Ventilated Photovoltaic Wall Panels. *Buildings* **2023**, *13*, 3002. https://doi.org/10.3390/buildings13123002

Academic Editor: Constantinos A. Balaras

Received: 26 October 2023
Revised: 17 November 2023
Accepted: 28 November 2023
Published: 30 November 2023

Copyright: © 2023 by the authors. Licensee MDPI, Basel, Switzerland. This article is an open access article distributed under the terms and conditions of the Creative Commons Attribution (CC BY) license (https://creativecommons.org/licenses/by/4.0/).

1. Introduction

With socio-economic development and a growing world population, problems such as fossil energy scarcity and global climate change are becoming increasingly serious. Solar energy is the most abundant resource on earth, and the introduction of photovoltaic technology has enabled solar energy to be effectively used for power generation and the heating of buildings [1]. The International Energy Agency (IEA) states that photovoltaic technology could provide approximately 25% of the global electricity by 2050 [2]. Moreover, the International Renewable Energy Agency (IRENA) predicts that about 32 billion tons of carbon dioxide emissions related to buildings will be offset annually by 2050 through the use of renewable energy sources [3]. Photovoltaic building integration is one of the technologies that significantly increase the share of renewable energy in building envelopes. PV facades are becoming an important component of PV building integration due to their great potential for solar energy applications in urban environments [4,5].

With the advancement of solar cell technology, 20% of the solar irradiation (SI) received by crystalline-silicon-type PV panels can be converted into electricity, and the rest of the solar radiation is accumulated inside the PV panels in the form of heat energy [6]. When photovoltaic panels are integrated into building facades, the heat generated by the solar cells

cannot be dissipated in a timely manner, resulting in higher cell temperatures. According to the literature, with every 1 °C increase in the cell temperature, its photoelectric conversion efficiency decreases by 0.4–0.5% [7,8]. Uneven operating temperatures and hot spots not only accelerate the heat loss of solar cells and shorten their service life [9–11], but they also lead to an increase in the temperature of the facade, which increases the cooling energy consumption for the building [12,13]. In addition, PV panels operating at high temperatures can cause thermal stresses on the facade, potentially damaging its internal structure [14]. The annual heat released from PV panels into the environment causes the ambient temperature to increase by 0.024 °C, which is one of the factors contributing to global warming [15,16].

Currently, cooling methods for PV cells can be broadly categorized into five types: passive cooling techniques, active cooling techniques, heat pipe cooling, nanofluid cooling, and thermoelectric cooling [17,18]. When PV panels are integrated into a building facade in the form of unit modules, it is common practice to reserve an air-cooled channel between the PV panels and the building facade to solve the heat dissipation problem of the PV panels [19,20]. In the open-air-cooled channel, the PV cells can be cooled down via natural ventilation without equipment intervention, or via mechanical ventilation using fans [21].

Agathokleous et al. [22] summarized a review of natural- and mechanical-ventilation systems for building-integrated photovoltaic (BIPV) systems, indicating that most scholars have focused on studying the mechanical-ventilation system, which can flexibly regulate the airflow in the air-cooled channel and facilitate experimental tests. In order to enhance the cooling effect of mechanical ventilation, Yasaman et al. [23] considered integrating an air diffuser with a deflector into PV panels to distribute the airflow uniformly. In addition, recent studies have proposed the incorporation of some heat dissipation structures on the backsides of PV panels. For example, Laura et al. [1] analyzed a BIPV system fitted with vertical heat dissipation fins, and this strategy resulted in a reduction in the PV-panel temperature by 5.2 °C and an increase in the annual energy production of 1.2%. Zeynep et al. [24] investigated the cooling effect of monocrystalline silicon photovoltaic panels under air-cooled channels with different wind speeds and different geometries, and the results showed that the fin cooling channel has a better cooling effect compared to the flat cooling channel. Tao et al. [25] proposed four different air-cooled circulation methods for bifacial PV/thermal modules, and the results showed that the air-cooled method with a back-and-forth channel had the best heat collection, while the PV/thermal module with a lower side channel had the best electrical energy output. Khushbu et al. [26] conducted an optimization study of PV-panel air-cooled radiators in Dubai, UAE, to analyze the effects of different fin spacings, base plate thicknesses, fin heights, and fin thicknesses on the heat dissipation, and to determine the optimum geometrical parameters for the radiators. Yogesh et al. [27] investigated the heat collection performance of a PV thermal system at a constant velocity and showed that the addition of fins can increase the contact area between the PV panels and the air; the thermal efficiency gain of the system was 3% higher than that of the conventional PV/T system, and the electrical gain was 0.2% higher than that of the conventional PV/T system at a wind speed of 0.2 m/s. Zhonghua et al. [28] mounted cooling fins on the backsides of PV panels and measured the effects of three different sets of fins on the electrical and thermal performances of the PV panels. Thus, it is clear that fins play an important role in the study of mechanical ventilation for the cooling and heat dissipation of PV panels [29,30].

Mechanical ventilation plays an important role in experimental research, and the air-cooling method can well control the air velocity in the cavity. However, in the actual implementation of the project, the active ventilation equipment and control system are difficult to put into use in a large number of PV facades. The natural-ventilation method remains the main means of heat dissipation for PV panels in PV-facade projects due to its simple construction and easy installation. Lau et al. [31] modeled the buoyancy-driven flow of a BIPV system in an open channel and explored the effects of different inclination angles on the temperature and velocity fields in the cavity. Agathokleous et al. [32] conducted a

thermal analysis of a naturally ventilated BIPV system, analyzed the thermal characteristics of the BIPV system in both indoor and outdoor environments, and estimated the convective heat transfer coefficients for both conditions. Mohammed et al. [33] proposed a novel renewable energy system consisting of a solar chimney, PV panels, and a soil–air heat exchanger, and investigated the natural ventilation within the system via the thermal buoyancy alone. Benzarti et al. [34] inserted a twisted baffle into a naturally ventilated BIPV system and explored the role that it played in improving the heat dissipation of PV panels.

It is known from the above literature that mechanical ventilation can give a good cooling effect to PV panels, but because this method is difficult to implement in practical engineering, natural air cooling is still considered for use to cool down PV panels. At present, the air-cooled channel commonly used for heat dissipation in engineering applications is generally a flat-plate structure. In order to obtain better power generation and heat collection efficiency, this paper proposes a vertical arrangement of the heat dissipation fins in the flat-plate air-cooled channel of PV wall panels to form a finned air-cooled channel. By analyzing the air-cooled channel with different dimensional parameters, the changes in the temperature and velocity fields in the PV wall panel are investigated to provide a basis for optimizing the structural dimensions of the finned air-cooled channel.

2. System Description

The simulation and analysis of the naturally ventilated PV wall panels in this paper are based on a set of experiments conducted by Agathokleous et al. [32], which empirically referred to a naturally ventilated BIPV system consisting of four parts: polycrystalline silicon photovoltaic panels, flat-plate air-cooled channels, wooden walls, and Plexiglas panels on both sides. As shown in Figure 1, the working principle of PV-panel cooling is natural air cooling under the effect of thermal buoyancy. When the outer photovoltaic panels are irradiated by solar radiation, about 20% of the solar irradiation is converted into electrical energy, and the rest is converted into heat energy. The heat generated by the PV panels heats the cold air in the flat-plate air-cooled channel and, due to buoyancy, the heated air moves upward until it is discharged, and the cold air enters at the bottom of the naturally ventilated BIPV system to form natural ventilation. This natural-air-cooling method utilizes the air in the air-cooled channel to take away the heat from the PV panels, which reduces their temperature and improves the photovoltaic conversion efficiency of the PV cells.

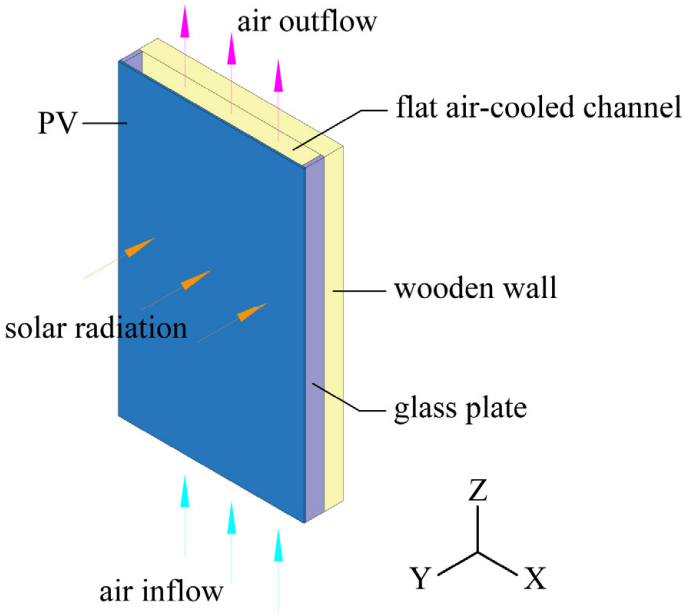


Figure 1. Structure of natural-ventilation building-integrated photovoltaic (BIPV) system.

Currently, natural air cooling is commonly used as the main form of cooling for PV panels in actual projects; however, the cooling effect of the traditional natural-air-cooling method on PV panels is not significant. Because heat dissipation fins can enhance the heat exchange effect between the air in the air-cooled channel and the PV panels, this paper considers installing rectangular fins vertically in the flat-plate air-cooled channel of the natural-ventilation BIPV system.

The naturally ventilated PV wall panel with fins, as shown in Figure 2a, is obtained by vertically installing a plurality of uniformly arranged rectangular fins within the flat-plate air-cooled channel of the naturally ventilated BIPV system shown in Figure 1. The fins divide the flat-plate air-cooled channel of Figure 1 into a plurality of finned air-cooled channels with repeating unit characteristics, as shown in Figure 2b. The top and bottom of the finned air-cooled channel are connected to the outside, with the air-cooled channel's inlet located at the bottom and its outlet positioned at the top. In this study, a CFD simulation model was used to simulate and analyze the dimensional parameters of the two types of air-cooled channels mentioned above. The study also investigated the variations in these channels under different levels of solar irradiation.

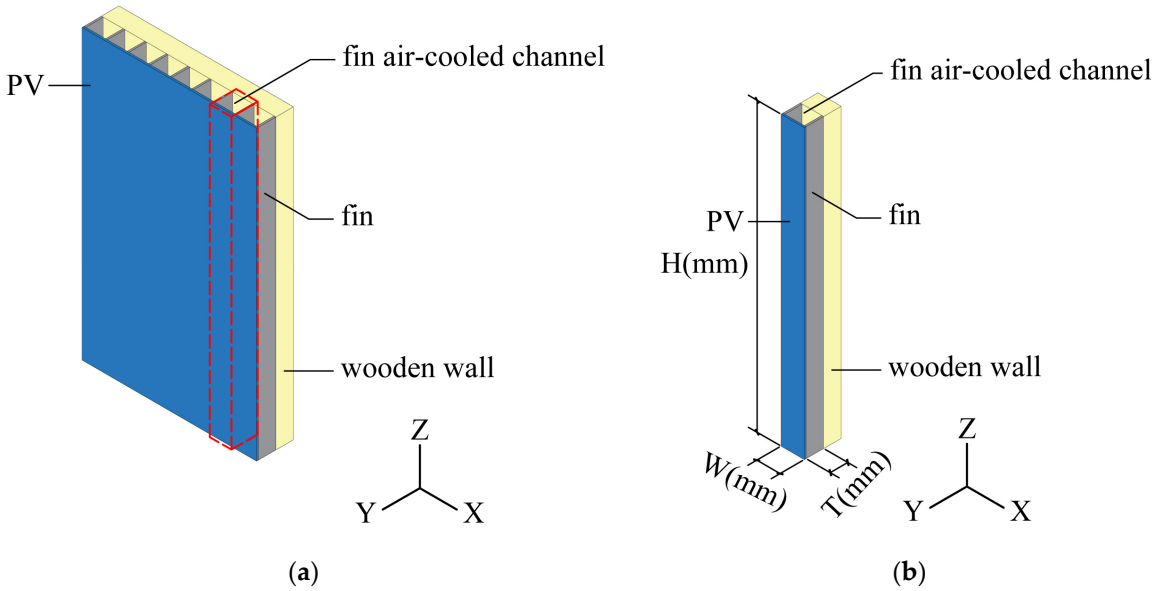


Figure 2. Structure of a natural-ventilation-type photovoltaic (PV) wall panel with vertically mounted rectangular fins: (**a**) complete model; (**b**) typical unit.

3. Methodology

In this study, the Fluent analysis system in Workbench was used for the CFD numerical-simulation method. The CFD numerical simulation was used to compare and analyze the temperature distribution and velocity distribution of the two different air-cooled-channel forms in Section 2 under various size parameters. In order to enhance the efficiency of the CFD numerical analysis, the CFD simulation of the finned air-cooled channel only involved simulating one unit, as shown in Figure 2b.

3.1. Geometry Model

Based on the two air-cooled-channel forms described in the previous section, their geometrical models were established. In this study, the air-cooled channels of the two aforementioned structures with different dimensional parameters were simulated separately. Design Modeler in ANSYS was utilized to create the geometric models. The material parameters are shown in Table 1.

Table 1. Material parameters of natural-ventilation-type PV wall panels.

Geometry	Height (mm)	Width (mm)	Thickness (mm)	Density (kg/m^3)	Thermal Conductivity (W/(m·K))	Specific Heat Capacity (J/(kg·K))
Photovoltaic panels	1642	992	4	1500	0.36	1760
Wooden wall	1642	992	100	2000	0.46	1500
Air-cooled channel	1642	992	100	1.177	0.0242	1006.43
Vertical fins (aluminum)	1642	100	2	2719	202.4	871

3.2. Mesh Generation

In order to obtain a high-quality computational mesh, the multizone was used as the mesh generation method for both the solid and fluid regions in the meshing setup, the mapped network type was hexahedral, and the minimum edge length was set to 1.0 mm. Mesh encryption was applied to the fluid–solid interface in the fluid region, with the maximum layers set to 5 and a growth rate of 1.2. The mesh physics preference was set to CFD, the solver preference was set to Fluent, and the minimum cell size was 5.0 mm. Because only one structural unit of the air-cooled channel in the ventilated PV wall panel in Section 3.1 was modeled, a symmetry plane was set for the model during the meshing. In addition, the lower boundary of the fluid domain was set as the inlet boundary, and the upper boundary of the fluid domain was set as the outlet boundary. The mesh model of the naturally ventilated PV wall panel based on the above mesh settings is shown in Figure 3. In this case, the maximum grid skewness is 0.51246, and the minimum orthogonal mass is 0.7011, which satisfies the accuracy required for grid quality.

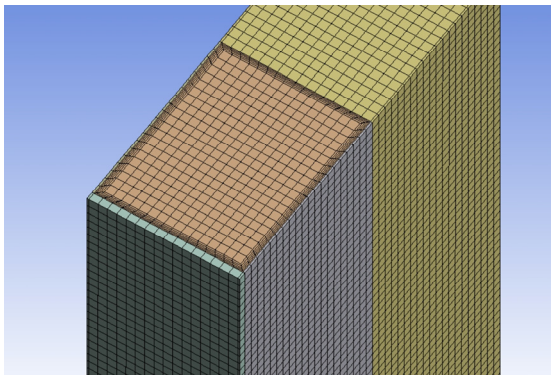


Figure 3. Grid model.

3.3. Grid Independence Verification

The simulations were carried out using five different minimum cell sizes: 5 mm, 10 mm, 15 mm, 20 mm, and 25 mm, to compare the average PV temperatures (T_{pv}) calculated in all cases, as shown in Table 2. The results show that, at a minimum cell size of 5 mm, the results calculated from its grid reached relative stability.

Table 2. Variation in simulation results with number of grids.

Basic Photovoltaic Wallboard		Photovoltaic Wallboard with Fins	
Grid Numbers	**T_{pv} (°C)**	**Grid Numbers**	**T_{pv} (°C)**
3400	63.92	5750	62.98
4712	63.76	9672	62.86
11,316	63.62	20,500	62.75
28,536	63.60	47,970	62.72
192,864	63.59	270,108	62.70

3.4. Assumptions

Agathokleous et al. [32] conducted a real measurement of a naturally ventilated BIPV system for 160 min, and its measured results reached a steady state within this time period; thus, the system underwent a process of shifting from a transient to steady state. In this study, the transient simulation of a naturally ventilated PV wall panel was analyzed, and its simulation results were compared with the measured data to verify the accuracy of the model. A thermal analysis of the different sizes of air-cooled channels in the naturally ventilated PV wall panel was performed to compare the simulation results when the model reached a steady state.

Based on this, the following assumptions were made in the Computational Fluid Dynamics (CFD) simulations:

The incident solar irradiation was considered to shine vertically on the outer surface of the PV panels. The air inside the air-cooled channel was considered as natural ventilation under thermal pressure. It was assumed that all the thermophysical parameters were constant except for the air density. The Boussinesq method was used for the air density, and the corresponding equation is written in Equation (1), where ρ_{amb} is the air density at ambient temperature (T_{amb}), and β is the coefficient of thermal expansion:

$$(\rho - \rho_{amb}) = -\rho_{amb}\beta(T - T_{amb}) \tag{1}$$

3.5. Governing Equation

In the CFD simulation analysis of naturally ventilated PV wall panels, considering the above assumptions, the Navier–Stokes equations were as follows:

The continuity equation is written in Equation (2), where $\vec{V_f}$ refers to the velocity:

$$\frac{\partial \rho_f}{\partial t} + \nabla \cdot \left(\rho_f \vec{V_f} \right) = 0 \tag{2}$$

The momentum equation is written in Equation (3), where $\vec{V_f}$, p, $\bar{\bar{\tau}}$, and g refer to the velocity, pressure, stress tensor, and gravitational acceleration, respectively:

$$\frac{\partial}{\partial t}\left(\rho_f \vec{V_f} \right) + \nabla \cdot \left(\rho_f \vec{V_f} \vec{V_f} \right) = -\nabla \mathrm{p} + \nabla \cdot \left(\bar{\bar{\tau}} \right) + \rho_f \vec{g} \tag{3}$$

The heat transfer process in the fluid field within an air-cooled channel is a combination of convection and conduction. However, in the solids (PV panels, fins, and walls), the heat transfer processes are conductive and radiative. Therefore, the energy equations for the fluid and solid regions are written in Equations (4) and (5), where the subscripts "s" and "f" denote solids and fluids. K and S_h are the thermal conductivity and heat source, respectively, indicating the amount of solar radiation absorbed by each solid layer:

$$\rho_f C_{P \cdot f} \left[\frac{\partial T_f}{\partial t} + \left(\vec{V_f} \cdot \nabla \right) T_f \right] = k_f \nabla^2 T_f \tag{4}$$

$$\rho_s C_{P \cdot s} \frac{\partial T_s}{\partial t} = k_s \nabla^2 T_s + S_h \tag{5}$$

The buoyancy-driven airflow in an air-cooled channel is described using the RNG k-epsilon model. This model provided good algorithms for the problem under consideration [35]. In this numerical simulation, the discrete-ordinate (DO) radiation model was used [36].

3.6. Boundary Conditions

For the air-cooled channel, the inlet boundary condition was set to the pressure inlet, the inlet pressure to ambient pressure, and the inlet temperature to ambient temperature.

The outlet boundary condition was set as the pressure outlet, the pressure was ambient pressure, and the temperature was ambient temperature.

No-slip boundary conditions were used for all the wall surfaces in the considered region. Mixed boundary conditions (convective heat transfer and radiative heat transfer) were set on the outer surface of the PV module. The natural convective heat transfer coefficient (h_{out}) between the PV panel and the environment is expressed by Equation (6) [37], where v_{wind} is the ambient wind speed:

$$h_{out} = 2.8 + 3.0v_{wind} \quad (6)$$

The temperature of the external radiation was considered as the sky temperature (T_{sky}), which is expressed by Equation (7) [38], where T_{amb} is the ambient temperature:

$$T_{sky} = 0.0522T_{amb}^{1.5} \quad (7)$$

The solar irradiation absorbed by the PV cells was considered as the heat generation source term in the PV panels.

3.7. Solution Method

In this study, the continuity, momentum, and energy equations were solved using the double-precision version of the commercial CFD package ANSYS Fluent computational tool. Based on the above assumptions, the finite-volume method was employed using the SIMPLE coupled pressure–velocity solver for mass conservation. Convective, diffusive-radiation, and turbulence terms were discretized using "second-order windward" discretization, and the pressure was solved using the PRESTO algorithm. The convergence criteria for the continuity, momentum, k-epsilon, and DO equations were set to 10^{-3}, and the energy equation was set to 10^{-6}. The maximum number of iteration steps was set to 2000.

3.8. Model Validation

In order to verify the reliability of the CFD numerical model in this paper, the simulation results were compared and verified with the measured results of the naturally ventilated BIPV system studied by Agathokleous et al. [32]. Because this paper focuses on the thermal analysis of air-cooled channels with different sizes of naturally ventilated photovoltaic wall panels, the measured data of the temperature points in the air-cooled channels were compared with the simulation results, and the comparison results are shown in Figure 4.

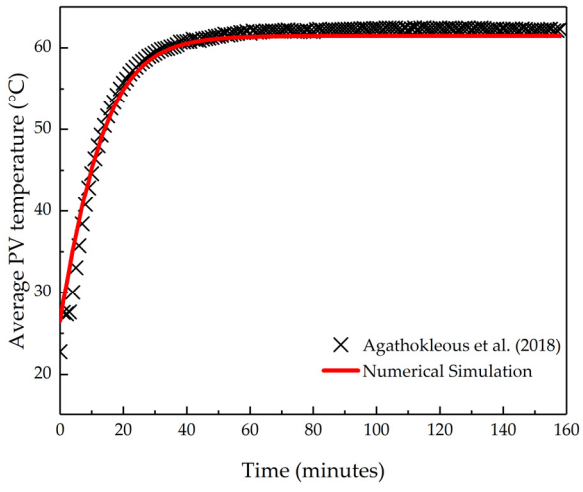


Figure 4. Comparison results between numerical-simulation and experimental data.

The validation studies were carried out in accordance with ASHRAE guideline 14 for energy measurements, which uses two criteria to define the numerical model's uncertainty: the Normalized Mean Bias Error (NMBE) and the Coefficient of Variation of Root Mean Square Error (CVRMSE). The corresponding equations are given in Equations (8) and (9), where y_s is the numerical-simulation value, y_{ref} is the experimental-measurement value, $\overline{y}_{ref}$ is the average of the measured values, and n is the number of measurements:

$$NMBE = \sum_{i=1}^{n} \left(y_{s(i)} - y_{ref(i)} \right) / \left(\overline{y}_{ref} \times n \right) \times 100 \quad (8)$$

$$CVRMSE = \left[\sqrt{\sum_{i=1}^{n} \left(y_{s(i)} - y_{ref(i)} \right)^2 / n} \right] / \overline{y}_{ref} \times 100 \quad (9)$$

From Figure 4, it can be seen that the simulation results are in good agreement with the experimentally measured parameters. The NMBE and CVRMSE values of the PV-panel surface temperature are −0.79% and 1.93%, respectively, which are within the acceptable calibration range of ASHRAE guideline 14. Therefore, the CFD simulation model proposed in this paper is validated and its simulation results can be used as a basis for the study of naturally ventilated PV wall panels.

4. Results and Discussion

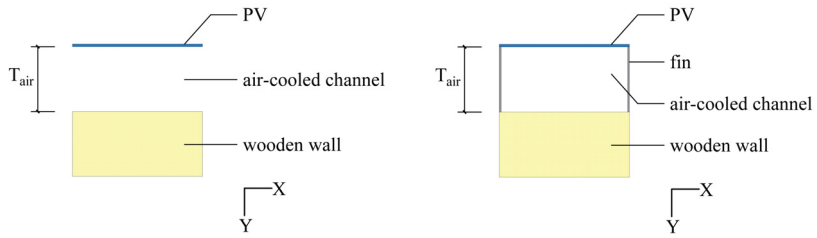
In this paper, the geometric parameters of air-cooled channels in natural-ventilation-type PV wall panels are investigated. The vertically arranged cooling fins separate the flat-plate air-cooled channel shown in Figure 1 into a number of finned air-cooled channels, as shown in Figure 2. To show the simulation content more clearly in this paper, the parameters of the simulation cases are shown in Table 3. The thicknesses of the air-cooled channels in Table 3 indicate the spacing between the PV panel and the wooden wall, and the widths of the air-cooled channels indicate the distance between the fins. Because the flat-plate air-cooled channel does not contain fins, there is no width of the air-cooled channel in Case 1. The simulation work was divided into three groups. Group 1 included Case 1 and Case 2, which were used to analyze the effects of flat-plate and finned air-cooled channels on naturally ventilated PV wall panels with different thickness parameters. Group 2 included Case 3, Case 4, and Case 5, which were used to analyze the effects of finned air-cooled channels with different widths on PV wall panels under three thickness parameters. Group 3 included Case 6 and Case 7, which were used to analyze the effects of flat-plate and finned air-cooled channels on PV wall panels under different levels of solar irradiance.

Table 3. Parameters of simulation cases.

Simulated Conditions	Case	Air-Cooled-Channel Thicknesses (mm)	Air-Cooled-Channel Widths (mm)	Solar Irradiance (W/m^2)	Ambient Temperature (°C)
Group 1	Case 1	40, 60, 80, 100, 120, 140, 160, 180, 200	-	800	25
	Case 2	40, 60, 80, 100, 120, 140, 160, 180, 200	80		
Group 2	Case 3	40	20, 40, 60, 80, 100, 120	800	25
	Case 4	100	20, 40, 60, 80, 100, 120		
	Case 5	180	20, 40, 60, 80, 100, 120		
Group 3	Case 6	100	-	200, 400, 600, 800	25
	Case 7	100	20	200, 400, 600, 800	

4.1. Study on Different Thicknesses of Air-Cooled Channels

The vertical installation of cooling fins in natural-ventilation-type PV wall panels can further enable the cold air in the air-cooled channel to exchange heat with the PV panels and take it away. In order to study the changes in the temperature and velocity fields of flat-plate and finned air-cooled channels under different thickness parameters, their corresponding numerical models were established. Figure 5a shows the naturally ventilated PV wall panels without heat dissipation fins, and Figure 5b shows the naturally ventilated PV wall panels with vertically mounted heat dissipation fins. The simulations were carried out for the cases in which the air-cooled-channel thicknesses (T_{air}) were 40 mm, 60 mm, 80 mm, 100 mm, 120 mm, 140 mm, 160 mm, 180 mm, and 200 mm. For the geometrical parameters of the finned air-cooled channel, the value of the width of the fins (W_{fin}) is the same as the value of the thickness of the air-cooled channel (T_{air}).



(**a**) (**b**)

Figure 5. Schematic diagrams of geometrical parameters of air-cooled channels: (**a**) flat-plate air-cooled channels; (**b**) finned air-cooled channels.

4.1.1. The Temperature Distribution of BIPV System

Figure 6 shows the temperature field for flat-plate and finned air-cooled channels with thicknesses of 40 mm and 100 mm. By comparing the temperature clouds (a) and (b), it can be seen that the installation of cooling fins can increase the air temperature around the fins. By comparing the temperature cloud diagrams (a) and (c), it can be seen that the air in the narrower air-cooled channel is heated more sufficiently, and therefore the buoyancy of the air is more intense. From Figure 6e,g, it can be seen that the narrower air-cooled channel has a limited flow of cold air, and the heated air reaches a higher temperature value before reaching the outlet of the air-cooled channel, which weakens the heat exchange between the air and the photovoltaic panels, and therefore the temperature on the surface of the photovoltaic panels near the outlet is at a higher level. A wider air-cooled channel provides more cold air, and the cold air close to the heated wall surface of the photovoltaic panels is sufficiently heated, while the cold air relatively far away from the heated wall surface is not heated. Therefore, the air in the channel is always at a lower temperature, and the air close to the exit still has a better cooling effect.

The peak temperatures in the air-cooled channels of the PV wall panels were analyzed because excessive local peak temperatures can damage the PV-panel components and affect their service life. Figures 7 and 8 show the temperature variations in the surface of the PV panels in the flat-plate and finned air-cooled channels when the thicknesses of the air-cooled channels were between 40 and 200 mm. As the thickness of the air-cooled channel increased, the maximum temperature value on the surface of the PV panels in the flat-plate air-cooled channel gradually decreased and reached a minimum at a thickness value of 100 mm, with insignificant changes thereafter, which is similar to the measured results of Agathokleous et al. [32] for this system. The average temperature of the PV-panel surface increased first with the thickness of the air-cooled channel and then decreased slowly, with the highest temperature at a thickness value of 140 mm.

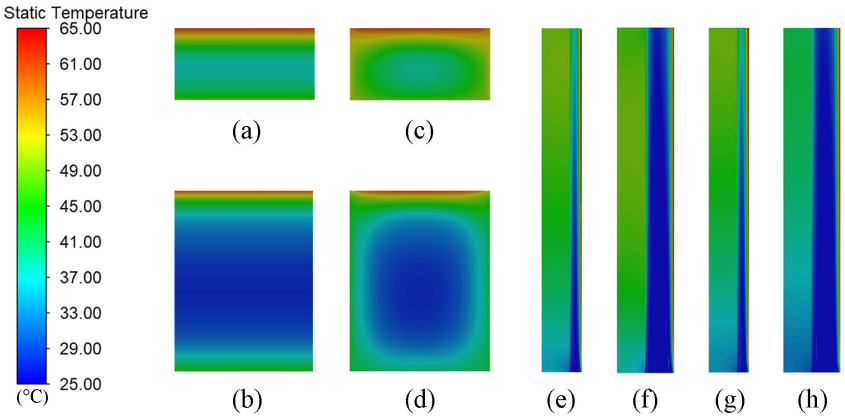


Figure 6. Temperature clouds of natural-ventilation-type PV wall panels: (**a**) outlet position of air-cooled channels for Case 1-T_{air}40; (**b**) outlet position of air-cooled channels for Case 1-T_{air}100; (**c**) outlet position of air-cooled channels for Case 2-T_{air}40; (**d**) outlet position of air-cooled channels for Case 2-T_{air}100; (**e**) side-section position of air-cooled channels for Case 1-T_{air}40; (**f**) side-section position of air-cooled channels for Case 1-T_{air}100; (**g**) side-section position of air-cooled channels for Case 2-T_{air}40; (**h**) side-section position of air-cooled channels for Case 2-T_{air} 100.

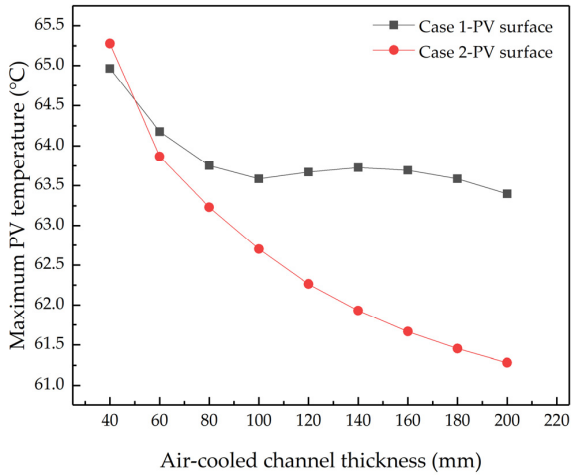


Figure 7. Comparison of the maximum surface temperatures of PV panels with different thicknesses of air-cooled channel.

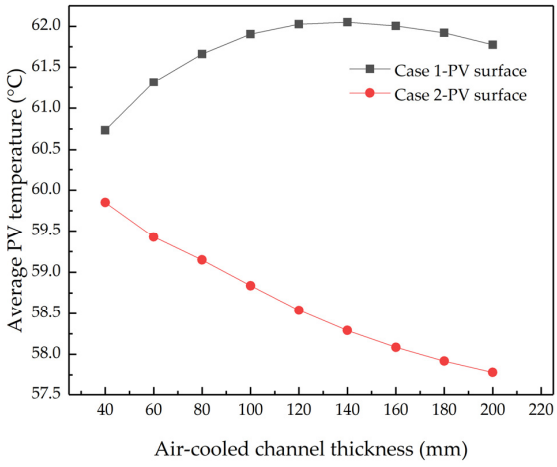


Figure 8. Comparison of the average surface temperatures of PV panels with different thicknesses of air-cooled channel.

As a result, the PV panels in the flat-plate air-cooled channel showed an increase in the average temperature at lower peak temperatures, resulting in some decrease in the electrical efficiency. Both the peak and average temperatures of the surface of the PV panels in the finned air-cooled channel decreased with the increase in the thickness of the air-cooled channel. Therefore, air-cooled channels fitted with cooling fins are beneficial for the lifetime and electrical efficiency of naturally ventilated photovoltaic wall panels compared to flat-plate air-cooled channels. When the width of the finned air-cooled channel was 80 mm and the thickness was 100 mm, the average and maximum temperatures on the surface of the photovoltaic panels decreased by 3.1 °C and 0.9 °C, respectively. When the width of the finned air-cooled channel was 80 mm and the thickness was 200 mm, the average and maximum temperatures of the surface of the PV panels decreased by 4 °C and 2.1 °C, respectively.

In order to further investigate the temperature distribution on the surface of the PV panels, temperature monitoring points were set every 20 mm along the height direction of the PV panels in the simulation. The temperature distributions on the surface of the PV panels with air-cooled-channel thicknesses of 40 mm, 100 mm, and 180 mm are shown in Figure 9. As can be seen from the figure, the overall temperature distribution in Case 2 is lower than that in Case 1, which indicates that the heat dissipation fins were able to improve the heat exchange between the PV panels and the cold air, which reduced the temperature on the surface of the PV panels. When the thickness of the air-cooled channel was 40 mm, the highest temperatures on the surface of the PV panels in Case 1 and Case 2 were obvious and both occurred at the exit of the PV wall panels. When the thicknesses of the air-cooled channel were 100 mm and 180 mm, the surface of the PV panels in Case 1 showed the obvious highest temperature, while Case 2 showed good temperature uniformity.

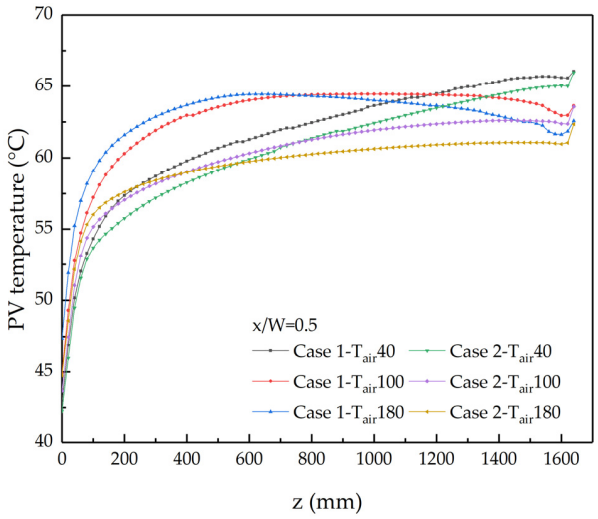


Figure 9. Comparison of temperature distributions along the height direction on the surface of photovoltaic panels with different thicknesses of air-cooled channel.

In addition, Figure 10 shows the variation in the air temperature in the air-cooled channel when the thickness was between 40 and 200 mm. From the figure, it can be seen that the average temperatures of the air inside the channel in Case 1 and Case 2 decreased as the thickness of the air-cooled channel increased, and the decrease gradually decreased. The air temperature inside the finned air-cooled channel was about 2 °C higher than that inside the flat-plate air-cooled channel, on average, indicating that the finned air-cooled channel is favorable for air heat collection. The air reached higher temperatures at the outlet, and the average temperature of the finned air-cooled channel at the outlet increased by more than 2 °C. As the thickness of the air-cooled channel increased, the average temperature at the outlet decreased; the decrease was not obvious when the thickness of the air-cooled channel exceeded 100 mm.

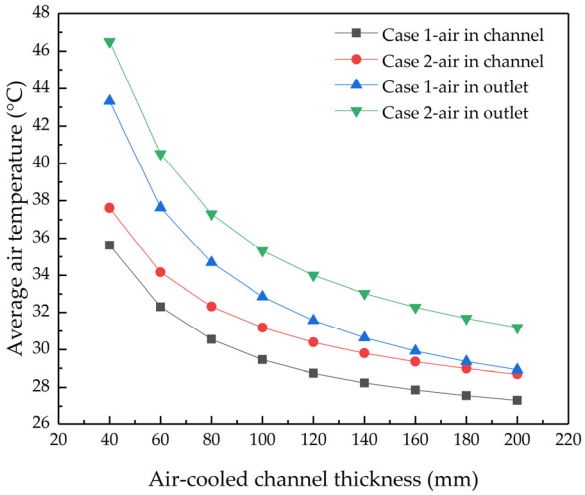


Figure 10. Comparison of air temperatures at different thicknesses of air-cooled channel.

Therefore, vertically mounted fins reduce the surface temperature of PV panels while promoting air heat collection in air-cooled channels. Narrower air-cooled channels are favorable for air heat collection, but, in this case, the PV panels are prone to higher peak temperatures. In order to avoid the high peak temperatures on the photovoltaic panel components that produce damage, a flat-plate air-cooled-channel thickness of 100 mm is preferred, and a finned air-cooled-channel thickness of 100 mm can further reduce the peak temperature.

4.1.2. Velocity Distribution of Air-Cooled Channels

As can be seen from Figure 11, vertically mounting the heat dissipation fins accelerates the airflow rate around the fins in the air-cooled channel. As the thickness of the air-cooled channel increases, the airflow rate in the channel shows an uneven distribution. The flow rate distribution shows that the airflow rate near the hot wall is fast.

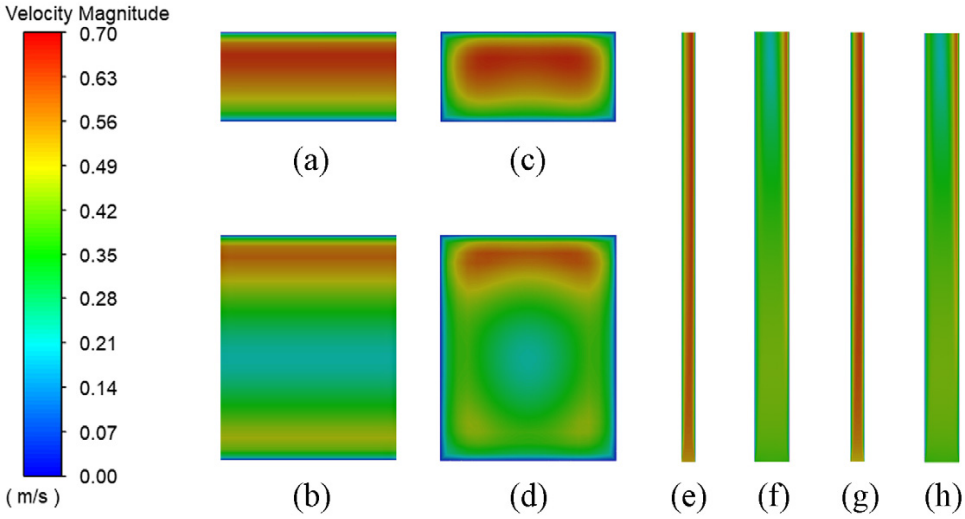


Figure 11. Velocity clouds of air-cooled channels in naturally ventilated PV wall panels: (**a**) outlet position of air-cooled channels for Case 1-T_{air}40; (**b**) outlet position of air-cooled channels for Case 1-T_{air}100; (**c**) outlet position of air-cooled channels for Case 2-T_{air}40; (**d**) outlet position of air-cooled channels for Case 2-T_{air}100; (**e**) side-section position of air-cooled channels for Case 1-T_{air}40; (**f**) side-section position of air-cooled channels for Case 1-T_{air}100; (**g**) side-section position of air-cooled channels for Case 2-T_{air}40; (**h**) side-section position of air-cooled channels for Case 2-T_{air}100.

Figures 12 and 13 show the variation in the flow velocity in the air-cooled channel for Case 1 and Case 2 between 40 mm and 200 mm. From the figures, it can be seen that as the thickness of the air-cooled channel increased, the average and maximum airflow rates decreased, which is due to the weakening of the air thermal buoyancy effect caused by more cold air. As the thickness of the air-cooled channel increased, the finned air-cooled channel showed better thermal buoyancy than the flat-plate air-cooled channel, which is due to the installation of heat dissipation fins to further heat the air inside the air-cooled channel.

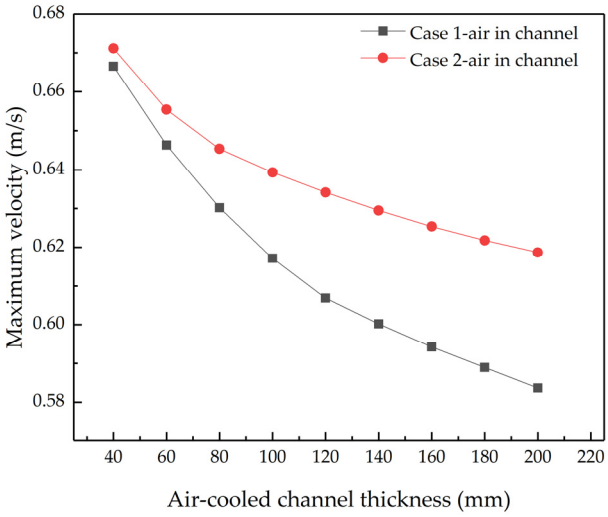


Figure 12. Comparison of maximum air velocity values for different thicknesses of air-cooled channel.

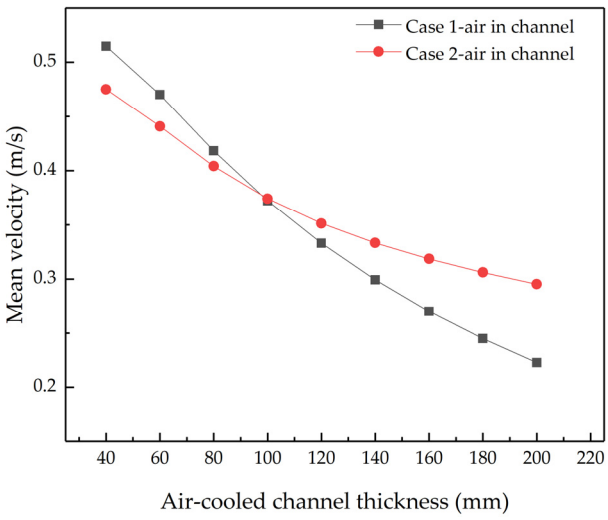


Figure 13. Comparison of average air velocity values for different thicknesses of air-cooled channel.

In order to further investigate the effect of the cooling fins on the airflow velocity in the air-cooled channel, the variations in the air velocity field in Case 1 and Case 2 are given for air-cooled-channel thicknesses of 40 mm, 100 mm, and 180 mm. Figure 14 shows the velocity distributions along the air-cooled-channel thickness direction at z/H = 0.25, 0.5, 0.75, 1, and x/S = 0.5. From the figure, it can be seen that the velocity in the channel is not uniformly distributed, the airflow velocity is fast at the place near the hot wall surface and slow at the place far away from the hot wall surface, and this feature is more obvious as the air is moved via thermal buoyancy along the height direction. As the thickness of the air-cooled channel increases, the overall airflow rate decreases. For the airflow rate in the middle of the channel, the finned air-cooled channel has a faster flow rate than the flat-plate air-cooled channel, which indicates that the installation of heat dissipation fins further

heats up the air in the air-cooled channel and enhances the overall thermal buoyancy of the air. As the thickness of the air-cooled channel becomes smaller, the thermal buoyancy of the air inside the channel becomes more obvious.

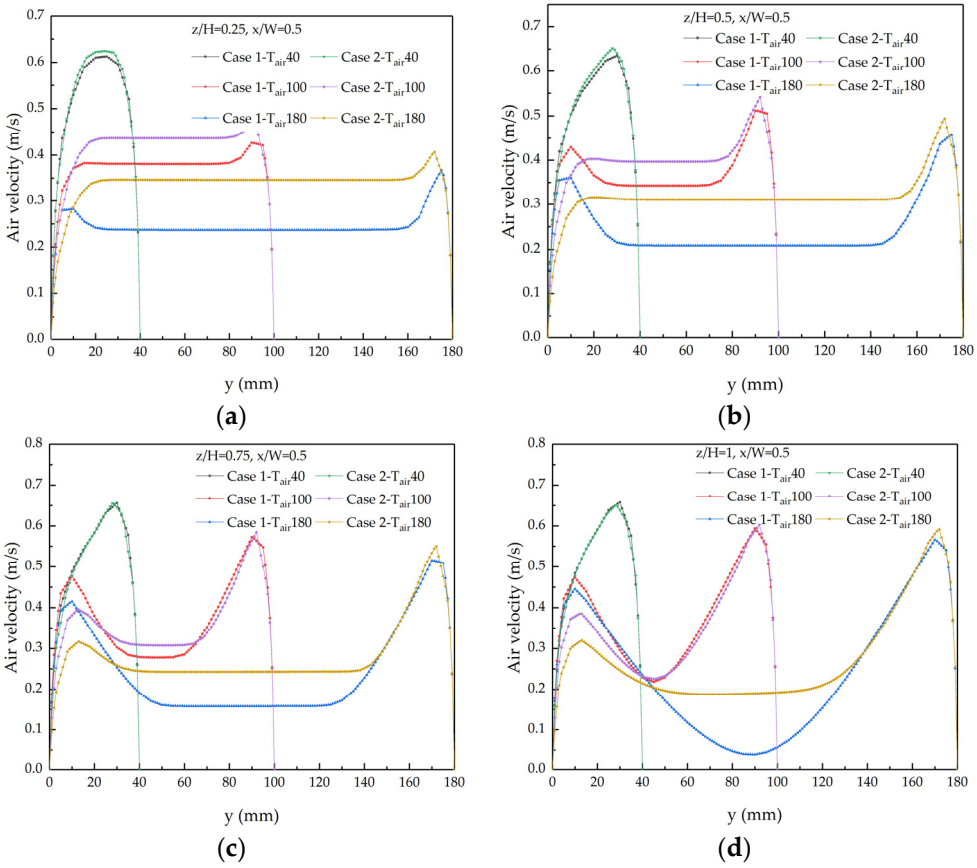


Figure 14. Comparison of air velocity distributions along the thickness direction of the air-cooled channel: (**a**) case located at z/H = 0.25, x/W = 0.5; (**b**) case located at z/H = 0.5, x/W = 0.5; (**c**) case located at z/H = 0.75, x/W = 0.5; (**d**) case located at z/H = 1, x/W = 0.5.

4.2. Study on Different Widths of Air-Cooled Channel

In this section, the temperature and velocity field variations in a finned air-cooled-channel width in the range of 20–120 mm for naturally ventilated PV wall panels are analyzed, and the geometrical models shown in Figure 15 are developed. The basic parameters of the cases are shown in Table 3, which were simulated with air-cooled-channel thicknesses of 40 mm, 100 mm, and 180 mm, and with widths of 20 mm, 40 mm, 60 mm, 80 mm, 100 mm, and 120 mm, respectively. For the geometrical parameters of the finned air-cooled channel, the value of the spacing of the fins (S_{fin}) is the same as the value of the width of the air-cooled channel (W_{air}).

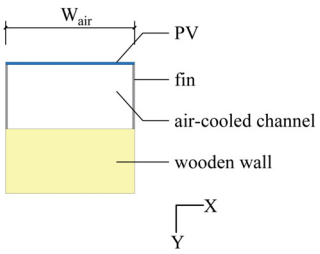


Figure 15. Schematic of the geometric parameters of the finned air-cooled channel in the naturally ventilated photovoltaic wall panels.

4.2.1. The Temperature Distribution of Air-Cooled Channels

Figure 16 shows temperature clouds for Case 4 at air-cooled-channel widths of 40 mm and 60 mm. From Figure 16a,c, it can be seen that the air temperature of the air-cooled channel at the exit was higher than that in the middle, and the air temperature was highest near the hot wall surface. As can be seen from Figure 16c,d, the air was heated more fully as the width of the air-cooled channel was reduced.

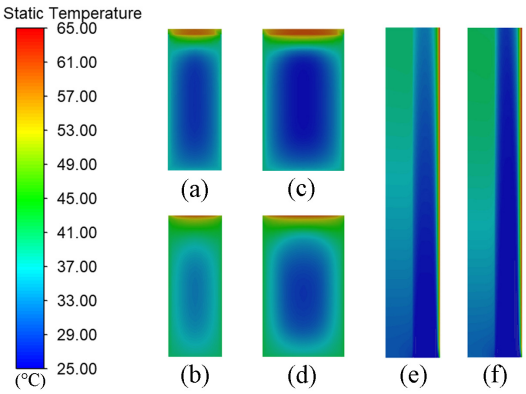


Figure 16. Temperature clouds of air-cooled channels in natural-ventilation-type PV wall panels: (**a**) middle position of air-cooled channels for Case 4-W_{air}40; (**b**) outlet position of air-cooled channels for Case 4-W_{air}40; (**c**) middle position of air-cooled channels for Case 4-W_{air}60; (**d**) outlet position of air-cooled channels for Case 4-W_{air}60; (**e**) side-section position of air-cooled channels for Case 4-W_{air}40; (**f**) side-section position of air-cooled channels for Case 4-W_{air}60.

The trend of the peak temperature on the surface of the PV panels is shown in Figure 17. For the case in which the thickness of the air-cooled channel is 40 mm, the smaller the width of the air-cooled channel, the higher the peak temperature on the surface of the PV panel. It can be seen from Section 4.1.1 that an air-cooled-channel thickness of 40 mm is insufficient to provide cold air, resulting in the air reaching a higher temperature before it reaches the outlet. At this point, a higher peak temperature occurs near the exit of the PV panel because the hot air becomes less capable of cooling it. For the cases with air-cooled-channel thicknesses of 100 mm and 180 mm, the maximum temperatures of the PV panels decrease with the reduction in the air-cooled-channel width, which is due to the fact that the thickness of the air-cooled channel is able to provide enough cold air, and the air inside the air-cooled channel still has a better cooling capacity despite the reduction in the air-cooled-channel width. In the above case, when the width of the air-cooled channel is between 60 and 120 mm, the maximum temperature of the surface of the PV panels does not change significantly, and the width of the air-cooled channel is within the range of 20–40 mm, which has a good heat dissipation effect.

The trend of the average temperature on the surface of the PV panel when the width of the air-cooled channel is from 20 mm to 120 mm is shown in Figure 18. For the case of an air-cooled-channel thickness of 40 mm, changing the air-cooled-channel width parameter has little effect on the average temperature of the PV-panel surface. For cases with air-cooled-channel thicknesses of 100 mm and 180 mm, changing the air-cooled-channel width parameter has a large effect on the average temperature of the PV-panel surface. As the width of the air-cooled channel increases, the surface temperature of the PV panels increases significantly, indicating that a finned air-cooled channel with a smaller width can transfer more heat from the PV panels to the air.

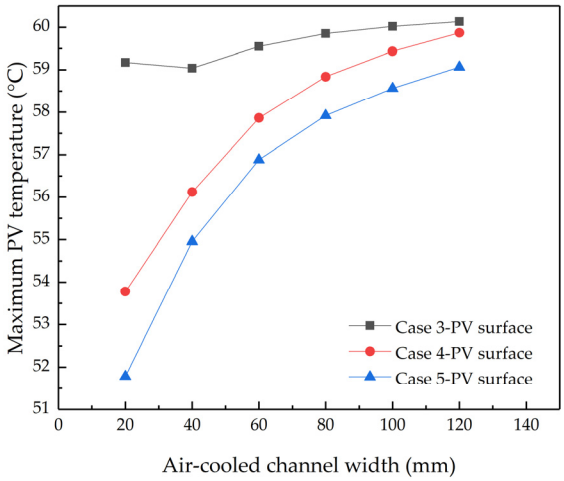


Figure 17. Comparison of maximum temperatures on the surface of photovoltaic panels with finned air-cooled channels of different widths.

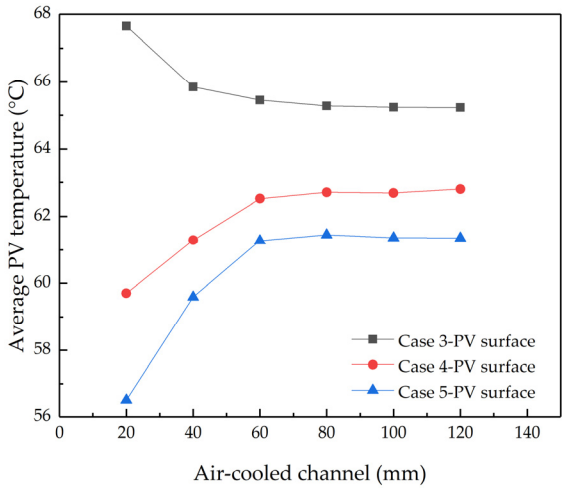


Figure 18. Comparison of average temperatures on the surface of PV panels with finned air-cooled channels of different widths.

Figure 19a,b show the temperature distributions on the surface of the photovoltaic panels when the thicknesses of the air-cooled channel were 40 mm and 100 mm, respectively. Firstly, compared with Case 1, the temperature of the PV-panel surface was reduced in both Case 3 and Case 4 due to the vertical installation of the heat dissipation fins. In addition, as can be seen from Figure 19a, in Case 3, due to the narrower air-cooled-channel thickness that could not provide sufficient cold air, a higher peak temperature was observed in the upper part of the PV-panel surface, whereas, in Figure 19b, the overall temperature on the surface of the PV panel decreased as the width of the air-cooled channel decreased due to the 100 mm thickness of the air-cooled channel.

Figure 20 shows the temperature variation in the air at an air-cooled-channel width from 20 to 120 mm. From the figure, it can be seen that the average temperatures of the air in Case 3, Case 4, and Case 5 decreased as the air-cooled-channel width parameter increased. In addition, compared to the PV wall panels with an air-cooled-channel thickness of 40 mm, the air-averaged temperature of the PV wall panels with an air-cooled-channel thickness of 100 mm increased by about 8 °C. When the air-cooled channel had a thickness of 100 mm and a width of 20 mm, the average temperature of the air increased by 5.6 °C compared to the width of 120 mm, which indicates that the air inside the air-cooled channel had a better cooling capacity under sufficient cold airflow, even though the width of the air-cooled channel was small.

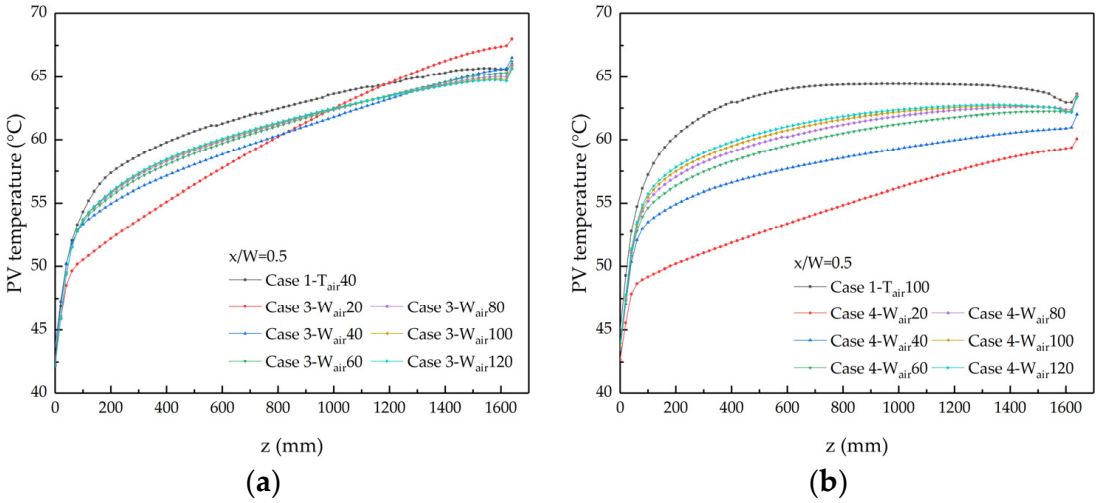


Figure 19. Comparison of temperature distributions along the height direction of the PV-panel surface: (**a**) Case 3; (**b**) Case 4.

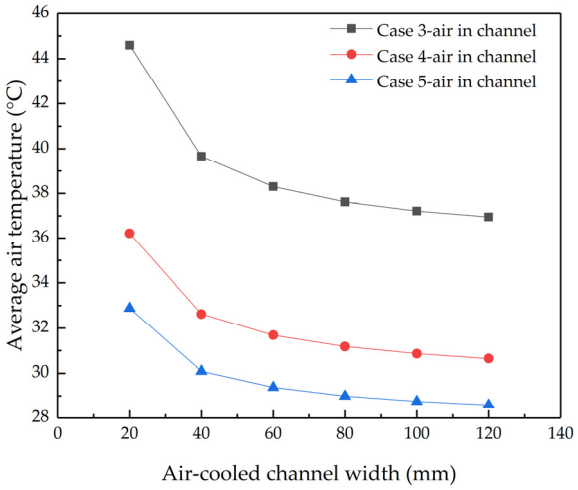


Figure 20. Comparison of average temperatures of the air in the channel at different widths of finned air-cooled channels.

Figure 21 shows the variation in the average temperatures of the air at the outlet for Case 3, Case 4, and Case 5 for air-cooled-channel widths from 20 to 120 mm. When the width of the air-cooled channel was less than 60 mm, the average temperature of the air significantly increased. Therefore, in order to pursue a better heat dissipation effect of PV panels, the thickness for the air-cooled channel that can provide a sufficient cold-air volume should be selected, along with a smaller air-cooled-channel width. In order to pursue a higher air heat collection effect, a smaller air-cooled-channel thickness should be selected, along with a smaller air-cooled-channel width.

4.2.2. Velocity Distribution of Air-Cooled Channels

Figure 22 shows the velocity clouds for the air-cooled-channel widths of 40 mm and 60 mm in Case 4, from which it can be seen that the airflow velocity is fast at the position close to the hot wall surface. With the smaller width of the air-cooled channel, the airflow velocity in the middle part of the air-cooled channel increases, which is due to the installation of fins, so that the air inside the channel away from the hot wall surface is heated, and the thermal buoyancy effect of the air is enhanced.

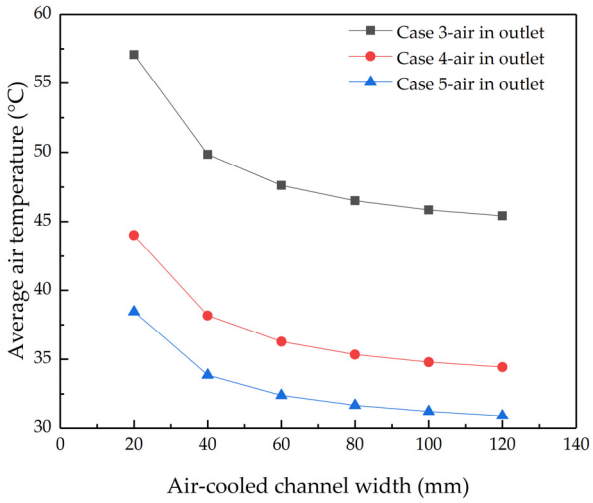


Figure 21. Comparison of average temperatures of air in outlet at different widths of finned air-cooled channels.

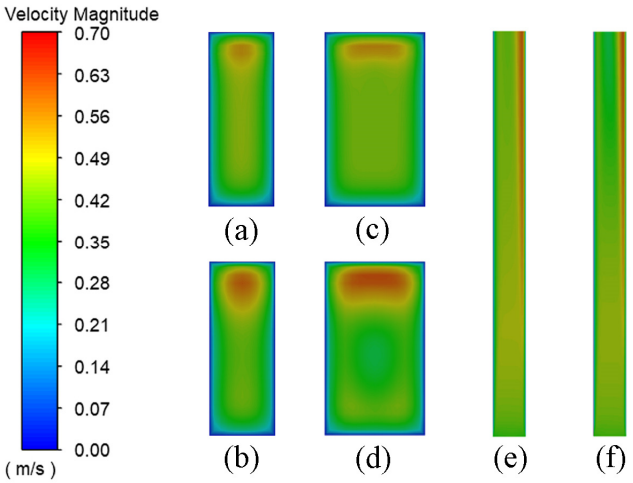


Figure 22. Velocity clouds of air-cooled channels of naturally ventilated PV wall panels: (**a**) middle position of air-cooled channels for Case 4-W_{air}40; (**b**) outlet position of air-cooled channels for Case 4-W_{air}40; (**c**) middle position of air-cooled channels for Case 4-W_{air}60; (**d**) outlet position of air-cooled channels for Case 4-W_{air}60; (**e**) side-section position of air-cooled channels for Case 4-W_{air}40; (**f**) side-section position of air-cooled channels for Case 4-W_{air}60.

For natural ventilation under thermal buoyancy, the larger the air temperature difference, the faster the airflow rate. Figures 23 and 24 show the variation in the airflow rates of air-cooled-channel widths between 20 and 120 mm for Case 3, Case 4, and Case 5. It can be seen in Figure 23 that the average airflow rate of Case 3 gradually increases with the increase in the air-cooled-channel width, and the average airflow rates of Case 4 and Case 5 first increase and then decrease. It can be seen in Figure 24 that Case 3, Case 4, and Case 5 have the lowest maximum velocity values when the width of the air-cooled channel is 20 mm, and the maximum velocity change is not obvious between 40 and 120 mm, which indicates that the temperature difference of the air inside the air-cooled channel is very small when the width is 20 mm, and the air is heated up sufficiently.

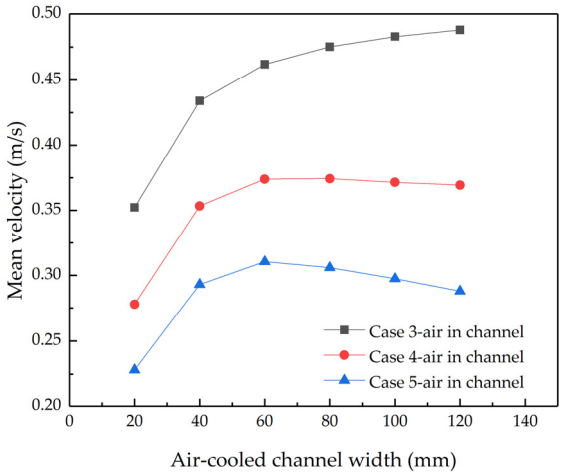


Figure 23. Comparison of average air velocities for different widths of finned air-cooled channels.

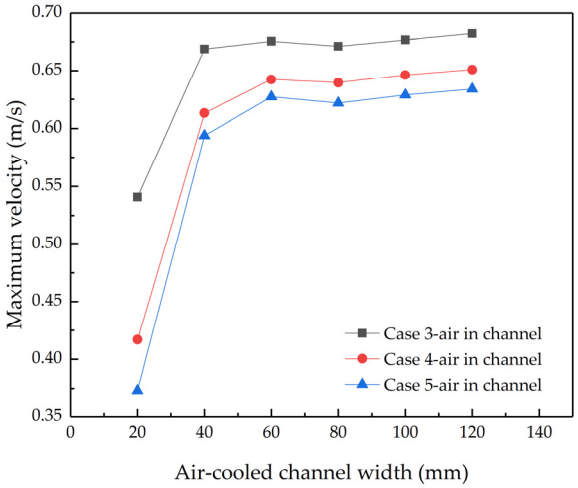


Figure 24. Comparison of maximum air velocities for different widths of finned air-cooled channels.

Figure 25 shows the air velocity field variations in the air-cooled channel in Case 4 for thicknesses ranging from 20 mm to 120 mm, where the measurement points are at z/H = 0.25, 0.5, 0.75, 1, and x/S = 0.5. From the figure, it can be seen that the air flows upward in the air-cooled channel due to the effect of the thermal buoyancy force, and the airflow velocity near the hot wall surface becomes faster, while the airflow velocity away from the hot wall surface becomes slower. Along the height direction, the peak airflow rate near the wall increases and the airflow rate away from the hot wall decreases. As the air away from the hot wall surface is heated by the fins, the airflow velocity increases in the region away from the hot wall surface as the fin spacing decreases.

4.3. Study on Different Solar Irradiations

The heat generation of the PV panels varies depending on the solar irradiation (SI) levels, and the air-cooled channel is also affected. In this section, Case 6 and Case 7 are analyzed at solar radiation intensities of 200 W/m^2, 400 W/m^2, 600 W/m^2, and 800 W/m^2, and the maximum temperatures on the surface of their PV panels are shown in Figure 26. As can be seen from the figure, the surface temperatures of the PV panels increased linearly with the solar irradiance within the solar radiation intensity range of 200–800 W/m^2. For every 200 W/m^2 increase in the solar radiation intensity, the maximum temperature of the PV-panel surface increased by about 8.4 °C for Case 6 and 7.4 °C for Case 7.

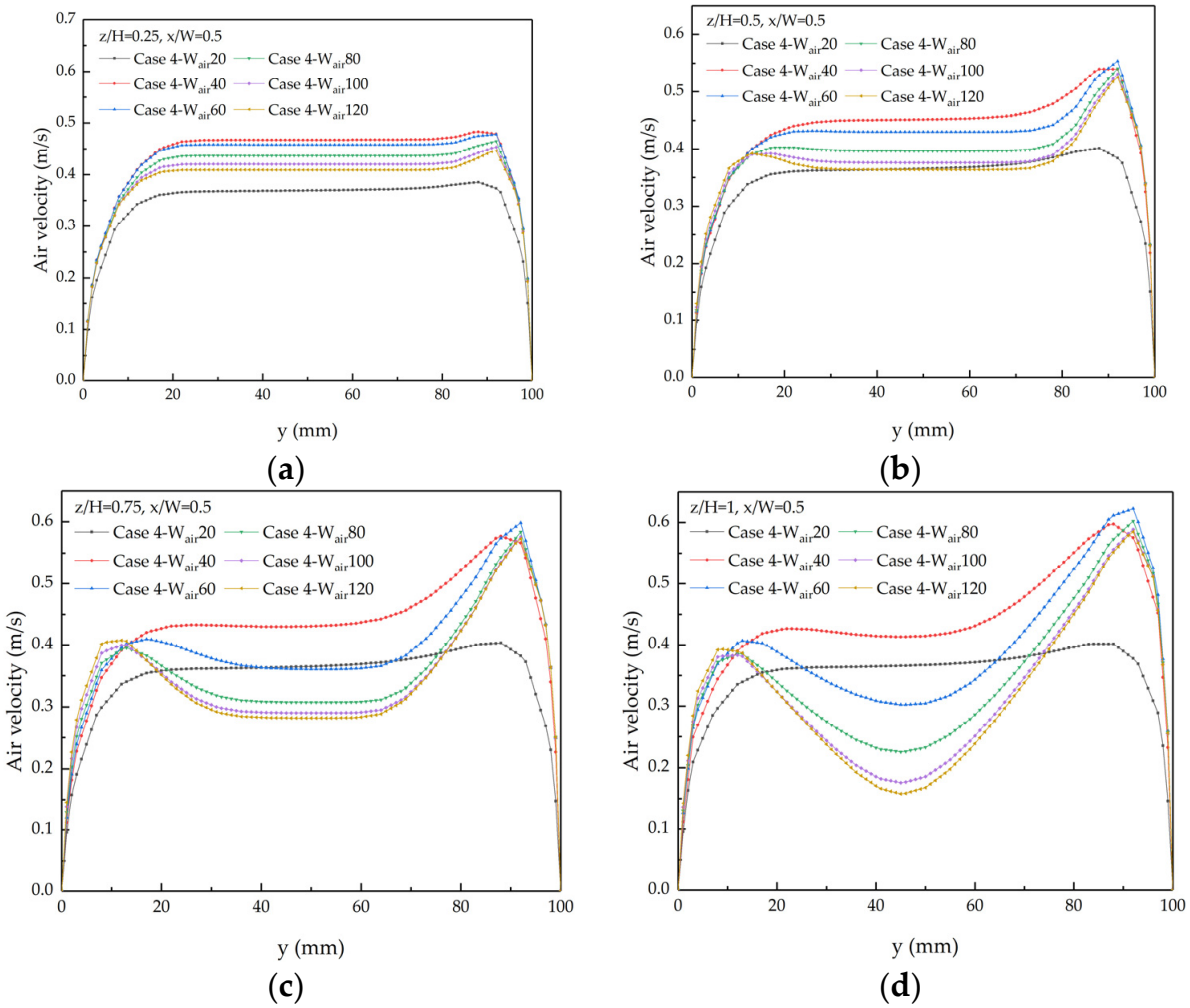


Figure 25. Comparison of air velocity distributions along the air-cooled-channel thickness direction: (**a**) case located at z/H = 0.25, x/W = 0.5; (**b**) case located at z/H = 0.5, x/W = 0.5; (**c**) case located at z/H = 0.75, x/W = 0.5; (**d**) case located at z/H = 1, x/W = 0.5.

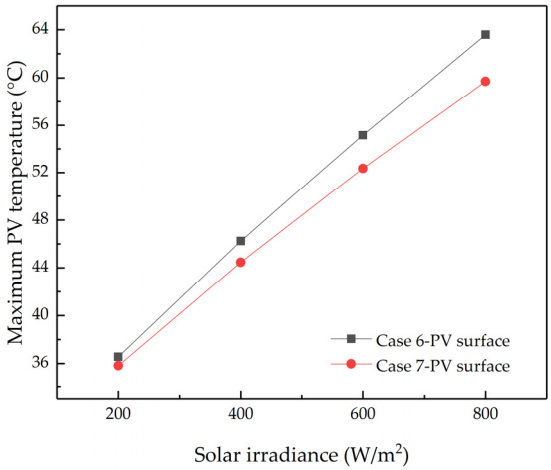


Figure 26. Comparison of the maximum temperatures of PV panels with different solar irradiations.

Figure 27 shows the average temperature changes on the surface of the PV panels in Case 6 and Case 7 when the solar radiation intensity distribution was 200 W/m^2, 400 W/m^2, 600 W/m^2, and 800 W/m^2. As can be seen from the figure, the surface temperature of the PV panel increased linearly with the solar irradiance within the solar radiation

intensity range of from 200 W/m^2 to 800 W/m^2. For every 200 W/m^2 increase in the solar radiation intensity, the average PV-panel surface temperature for Case 6 increased by 8.1 °C, and the maximum PV-panel surface temperature for Case 7 increased by about 6.2 °C. Figures 26 and 27 are sufficient to show that the finned air-cooled channel possesses a better cooling effect than the flat-plate air-cooled channel. According to the trend, the higher the intensity of solar radiation, the more obvious the cooling effect of the finned air-cooled channel.

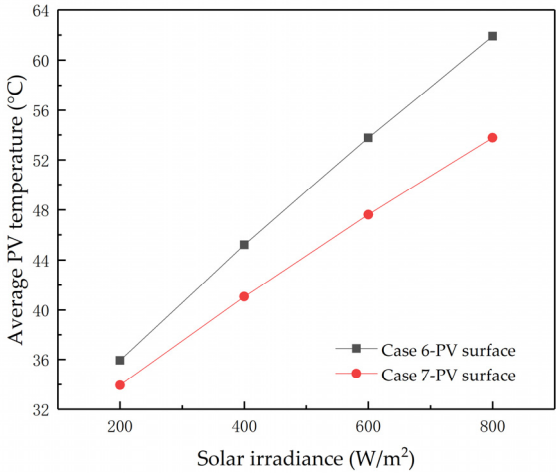


Figure 27. Comparison of average temperatures of PV panels with different solar irradiations.

In order to understand the PV surface temperature distributions of the above two air-cooled channels under different solar radiation intensities, a temperature monitoring point was set every 20 mm along the height direction of the PV panels; the temperature distribution graph is shown in Figure 28. As can be seen from the figure, at the solar radiation intensity of 200 W/m^2, the flat-plate-type and fin-type air-cooled channels maintained the PV-panel surface temperature at a lower level, and the temperature uniformity as well. At a solar radiation intensity of 800 W/m^2, the flat-plate and finned air-cooled channels had very high temperatures and poor temperature uniformities. As the intensity of the solar radiation increased, the finned air-cooled channel had a more significant cooling effect compared to the flat-plate air-cooled channel. Therefore, installing fins in the air-cooled channel can better enable the air cooling of PV wall panels under higher solar radiation.

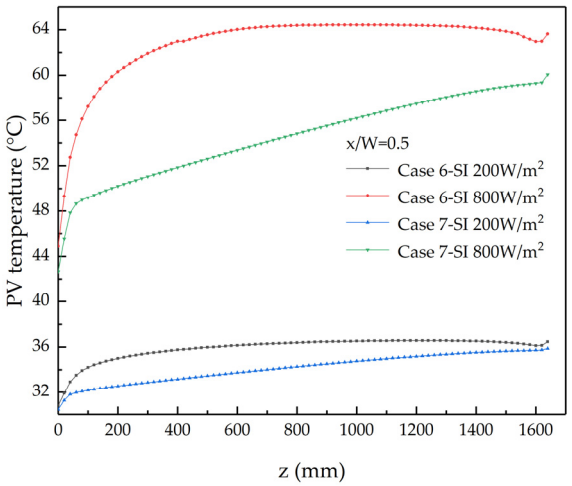


Figure 28. Comparison of temperature distributions along height direction on surfaces of photovoltaic panels with different solar irradiations.

Figure 29 shows the average temperature changes of the air inside the air-cooled channels for Case 6 and Case 7 at different solar radiation levels. From the figure, it can be seen that the average temperatures of the air inside the two air-cooled channels increased with the increase in the solar radiation intensity, and the finned air-cooled channel showed a better heat collection effect than the flat-plate air-cooled channel. When the intensity of the solar radiation was 200 W/m^2, the temperature difference between the two air-cooled channels was about 3 °C. When the solar radiation intensity was 800 W/m^2, the temperature difference between the two air-cooled channels was about 6.7 °C.

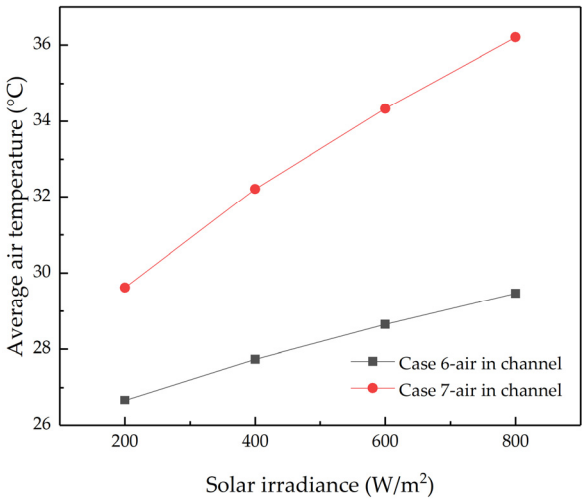


Figure 29. Comparison of average temperatures of air in channels with different solar irradiations.

Figure 30 shows the variations in the average air temperatures at the outlet of the air-cooled channels for Case 6 and Case 7 at different solar radiation intensities. From the figure, it can be seen that the trend of the average air temperature change at the exit is similar to that in Figure 29. When the solar radiation intensity was 200 W/m^2, the temperature difference between the two air-cooled channels was about 4.5 °C. When the solar radiation intensity was 800 W/m^2, the temperature difference between the two air-cooled channels was about 11.2 °C. Comparing the results of the data in Figures 29 and 30, it can be seen that the finned air-cooled channel had a better heat collection effect as the solar radiation intensity increased. Therefore, installing fins vertically in the air-cooled channel not only cools the PV panels better but also has a better air heat collection effect.

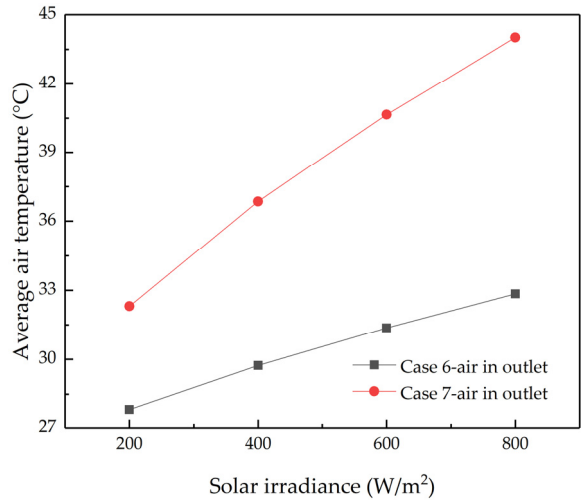


Figure 30. Comparison of average temperatures of air in outlet with different solar irradiations.

5. Conclusions

In this paper, the vertical installation of heat dissipation fins in the air-cooled channels of natural-ventilation-type PV wall panels is considered. The CFD numerical model of the natural-ventilation-type PV wall panels has been established and verified, and the temperature field and velocity field variations in the air-cooled channel with different size parameters have been analyzed. The conclusions of this study are as follows:

(1) Finned air-cooled channels provide enhanced cooling for PV panels. As the thickness of the finned air-cooled channel increases or the width decreases, the peak and average temperatures at the back of the PV panel decrease significantly. When the thickness of the finned air-cooled channel is 100 mm and the width is 20 mm, the maximum and average temperatures on the surface of the PV panels decrease by 3.9 °C and 8.1 °C, respectively, compared with the flat-plate air-cooled channel with a thickness of 100 mm;

(2) Finned air-cooled channels have a better air heat collection effect. As the thickness of the finned air-cooled channel decreases or the width decreases, the air temperature at the outlet of the air-cooled channel increases significantly. When the thickness of the finned air-cooled channel is 100 mm and the width is 20 mm, the average temperature of the air at the outlet increases by 11.2 °C compared with that of the flat-plate air-cooled channel with a thickness of 100 mm;

(3) In the flat-plate air-cooled channel, the airflow rate distribution shows that the flow rate is fast in the area near the hot wall and slow in the middle area of the air-cooled channel. The vertical installation of cooling fins will increase the airflow rate in the middle area of the air-cooled channel, and, as the width of the air-cooled channel becomes smaller, the airflow rate in the middle area will increase more obviously;

(4) Finned air-cooled channels have better photovoltaic-plate-cooling and air heat collection capacities than flat-plate air-cooled channels. With the increase in the solar radiation intensity, this trend becomes more obvious.

Author Contributions: Conceptualization, Y.Z., J.M. and H.Y; methodology, Y.Z.; software, Y.Z. and Q.C.; validation, J.M., H.Y. and F.L.; formal analysis, Y.Z.; investigation, J.M. and H.Y.; resources, J.M. and H.Y.; data curation, Y.Z.; writing—original draft preparation, Y.Z.; writing—review and editing, J.M., H.Y. and Y.Z.; visualization, Y.Z. and Q.C.; supervision, J.M.; funding acquisition, J.M. All authors have read and agreed to the published version of the manuscript.

Funding: Science and Technology SMEs Innovation Capacity Enhancement Project of Shandong Province (2022TSGC2144). Key Research and Development Program of Shandong (2018GSF122003).

Data Availability Statement: No new data were created.

Conflicts of Interest: The authors declare no conflict of interest.

References

1. Maturi, L.; Lollini, R.; Moser, D.; Sparber, W. Experimental investigation of a low cost passive strategy to improve the performance of Building Integrated Photovoltaic systems. *Sol. Energy* **2015**, *111*, 288–296. [CrossRef]
2. de Paulo, A.F.; Porto, G.S. Solar energy technologies and open innovation: A study based on bibliometric and social network analysis. *Energy Policy* **2017**, *108*, 228–238. [CrossRef]
3. Skočilas, J.; Palaziuk, I. CFD Simulation of the Heat Transfer Process in a Chevron Plate Heat Exchanger Using the SST Turbulence Model. *Acta Polytech.* **2015**, *55*, 267. [CrossRef]
4. Jäger-Waldau, A.; Kougias, I.; Taylor, N.; Thiel, C. How photovoltaics can contribute to GHG emission reductions of 55% in the EU by 2030. *Renew. Sustain. Energy Rev.* **2020**, *126*, 109836. [CrossRef]
5. Gonçalves, J.E.; van Hooff, T.; Saelens, D. Understanding the behaviour of naturally-ventilated BIPV modules: A sensitivity analysis. *Renew. Energy* **2020**, *161*, 133–148. [CrossRef]
6. Shahsavar, A.; Entezari, S.; Askari, I.B.; Ali, H.M. The effect of using connecting holes on heat transfer and entropy generation behaviors in a micro channels heat sink cooled with biological silver/water nanofluid. *Int. Commun. Heat Mass Transf.* **2021**, *123*, 104929. [CrossRef]
7. Mojumder, J.C.; Chong, W.T.; Ong, H.C.; Leong, K.; Mamoon, A.A. An experimental investigation on performance analysis of air type photovoltaic thermal collector system integrated with cooling fins design. *Energy Build.* **2016**, *130*, 272–285. [CrossRef]

8. Stodolny, M.K.; Janssen, G.J.; Van Aken, B.B.; Tool, K.C.; Lamers, M.W.; Romijn, I.G.; Venema, P.R.; Renes, M.R.; Siarheyeva, O.; Granneman, E.H.; et al. PID-and UVID-free n-type Solar Cells and Modules. *Energy Procedia* **2016**, *92*, 609–616. [CrossRef]
9. Liu, Z.; Zhang, L.; Gong, G.; Li, H.; Tang, G. Review of solar thermoelectric cooling technologies for use in zero energy buildings. *Energy Build.* **2015**, *102*, 207–216. [CrossRef]
10. Dash, P.; Gupta, N.; Rawat, R.; Pant, P. A novel climate classification criterion based on the performance of solar photovoltaic technologies. *Sol. Energy* **2017**, *144*, 392–398. [CrossRef]
11. Yang, T.; Braun, P.V.; Miljkovic, N.; King, W.P. Phase Change Material Heat Sink for Transient Cooling of High-Power Devices. *Int. J. Heat Mass Transf.* **2021**, *170*, 121033. [CrossRef]
12. Elghamry, R.; Hassan, H.; Hawwash, A. A parametric study on the impact of integrating solar cell panel at building envelope on its power, energy consumption, comfort conditions, and CO_2 emissions. *J. Clean. Prod.* **2020**, *249*, 119374. [CrossRef]
13. Peng, J.; Lu, L.; Yang, H.; Han, J. Investigation on the annual thermal performance of a photovoltaic wall mounted on a multi-layer façade. *Appl. Energy* **2013**, *112*, 646–656. [CrossRef]
14. Bahaidarah, H.M.; Baloch, A.A.; Gandhidasan, P. Uniform cooling of photovoltaic panels: A review. *Renew. Sustain. Energy Rev.* **2016**, *57*, 1520–1544. [CrossRef]
15. Hu, A.; Levis, S.; Meehl, G.A.; Han, W.; Washington, W.M.; Oleson, K.W.; van Ruijven, B.J.; He, M.; Strand, W.G. Strand. Impact of solar panels on global climate. *Nat. Clim. Chang.* **2016**, *6*, 290–294. [CrossRef]
16. Hosenuzzaman, M.; Rahim, N.A.; Selvaraj, J.; Hasanuzzaman, M.; Malek, A.B.M.A.; Nahar, A. Global prospects, progress, policies, and environmental impact of solar photovoltaic power generation. *Renew. Sustain. Energy Rev.* **2015**, *41*, 284–297. [CrossRef]
17. Siecker, J.; Kusakana, K.; Numbi, B. A review of solar photovoltaic systems cooling technologies. *Renew. Sustain. Energy Rev.* **2017**, *79*, 192–203. [CrossRef]
18. Nižetić, S.; Jurčević, M.; Čoko, D.; Arıcı, M. A novel and effective passive cooling strategy for photovoltaic panel. *Renew. Sustain. Energy Rev.* **2021**, *145*, 111164. [CrossRef]
19. Mirzaei, P.A.; Paterna, E.; Carmeliet, J. Investigation of the role of cavity airflow on the performance of building-integrated photovoltaic panels. *Sol. Energy* **2014**, *107*, 510–522. [CrossRef]
20. Saadon, S.; Gaillard, L.; Giroux-Julien, S.; Ménézo, C. Simulation study of a naturally-ventilated building integrated photovoltaic/thermal (BIPV/T) envelope. *Renew. Energy* **2016**, *87*, 517–531. [CrossRef]
21. Verma, S.; Mohapatra, S.; Chowdhury, S.; Dwivedi, G. Cooling techniques of the PV module: A review. *Mater. Today Proc.* **2021**, *38*, 253–258. [CrossRef]
22. Agathokleous, R.A.; Kalogirou, S.A. Double skin facades (DSF) and building integrated photovoltaics (BIPV): A review of configurations and heat transfer characteristics. *Renew. Energy* **2016**, *89*, 743–756. [CrossRef]
23. Amanlou, Y.; Hashjin, T.T.; Ghobadian, B.; Najafi, E.G. Air cooling low concentrated photovoltaic/thermal (LCPV/T) solar collector to approach uniform temperature distribution on the PV plate. *Appl. Therm. Eng.* **2018**, *141*, 413–421. [CrossRef]
24. Özcan, Z.; Gülgün, M.; Şen, E.; Çam, N.Y.; Bilir, L. Cooling channel effect on photovoltaic panel energy generation. *Sol. Energy* **2021**, *230*, 943–953. [CrossRef]
25. Ma, T.; Kazemian, A.; Habibollahzade, A.; Salari, A.; Gu, W.; Peng, J. A comparative study on bifacial photovoltaic/thermal modules with various cooling methods. *Energy Convers. Manag.* **2022**, *263*, 115555. [CrossRef]
26. Mankani, K.; Chaudhry, H.N.; Calautit, J.K. Optimization of an air-cooled heat sink for cooling of a solar photovoltaic panel: A computational study. *Energy Build.* **2022**, *270*, 112274. [CrossRef]
27. Agrawal, Y.; Mishra, A.; Gautam, A.; Phaldessai, G.; Yadav, A.S.; Vyas, M. Performance analysis of photovoltaic thermal air collector having rectangular fins. *Mater. Today Proc.* **2023**, *84*, 6–15. [CrossRef]
28. Zhao, Z.; Zhu, L.; Wang, Y.; Huang, Q.; Sun, Y. Experimental investigation of the performance of an air type photovoltaic thermal collector system with fixed cooling fins. *Energy Rep.* **2023**, *9* (Suppl. S4), 93–100. [CrossRef]
29. Ekoe, A.; Akata, A.M.; Njomo, D.; Agrawal, B. Thermal Energy Optimization of Building Integrated Semi-Transparent Photovoltaic Thermal Systems. *Int. J. Renew. Energy Dev.* **2015**, *4*, 113–123. [CrossRef]
30. Grubišić-Čabo, F.; Nižetić, S.; Čoko, D.; Kragić, I.M.; Papadopoulos, A. Experimental investigation of the passive cooled free-standing photovoltaic panel with fixed aluminum fins on the backside surface. *J. Clean. Prod.* **2018**, *176*, 119–129. [CrossRef]
31. Lau, S.-K.; Zhao, Y.; Shabunko, V.; Chao, Y.; Lau, S.S.-Y.; Tablada, A.; Reindl, T. Optimization and Evaluation of Naturally Ventilated BIPV Façade Design. *Energy Procedia* **2018**, *150*, 87–93. [CrossRef]
32. Agathokleous, R.A.; Kalogirou, S.A. Part I: Thermal analysis of naturally ventilated BIPV system: Experimental investigation and convective heat transfer coefficients estimation. *Sol. Energy* **2018**, *169*, 673–681. [CrossRef]
33. Alkaragoly, M.; Maerefat, M.; Targhi, M.Z.; Abdljalel, A. An innovative hybrid system consists of a photovoltaic solar chimney and an earth-air heat exchanger for thermal comfort in buildings. *Case Stud. Therm. Eng.* **2022**, *40*, 102546. [CrossRef]
34. Benzarti, S.; Chaabane, M.; Mhiri, H.; Bournot, P. Performance improvement of a naturally ventilated building integrated photovoltaic system using twisted baffle inserts. *J. Build. Eng.* **2022**, *53*, 104553. [CrossRef]
35. Arslan, E.; Aktaş, M.; Can, F. Experimental and numerical investigation of a novel photovoltaic thermal (PV/T) collector with the energy and exergy analysis. *J. Clean. Prod.* **2020**, *276*, 123255. [CrossRef]
36. Maadi, S.R.; Khatibi, M.; Ebrahimnia-Bajestan, E.; Wood, D. Coupled thermal-optical numerical modeling of PV/T module—Combining CFD approach and two-band radiation DO model. *Energy Convers. Manag.* **2019**, *198*, 111781. [CrossRef]

37. Li, M.; Ma, T.; Liu, J.; Li, H.; Xu, Y.; Gu, W.; Shen, L. Numerical and experimental investigation of precast concrete facade integrated with solar photovoltaic panels. *Appl. Energy* **2019**, *253*, 113509. [CrossRef]
38. Swinbank, W.C. Long-wave radiation from clear skies. *Q. J. R. Meteorol. Soc.* **1963**, *89*, 339–348. [CrossRef]

Disclaimer/Publisher's Note: The statements, opinions and data contained in all publications are solely those of the individual author(s) and contributor(s) and not of MDPI and/or the editor(s). MDPI and/or the editor(s) disclaim responsibility for any injury to people or property resulting from any ideas, methods, instructions or products referred to in the content.